An Examination of the Clear-Sky Solar Absorption over the Central Equatorial Pacific: Observations versus Models

WILLIAM C. CONANT, V. RAMANATHAN, AND FRANCISCO P. J. VALERO

Scripps Institution of Oceanography, University of California, San Diego, La Jolla, California

JENS MEYWERK

Meteorologisches Institution, Universität Hamburg, Hamburg, Germany

(Manuscript received 26 October 1995, in final form 23 October 1996)

ABSTRACT

Measurements of downward surface solar radiation (global radiation) and albedo taken during the Central Equatorial Pacific Experiment (CEPEX) are used to obtain baseline estimates for two quantities concerning the radiation budget of the tropical oceans: 1) surface absorption of solar radiation in the central equatorial Pacific under cloud-free conditions, and 2) the corresponding absorption by the atmosphere. These values are then compared to two state-of-the-art radiative transfer models to determine if the models are accurately partitioning solar absorption between the atmosphere and the ocean.

The paper develops an independent approach to obtain a clear-sky signal from 10-s resolution surface pyranometer data that is in excellent agreement with upper envelope methods. Over a diurnal average, the ocean absorbs 70.9% ± 1.3% of the solar radiation incident at the top of the atmosphere (TOA). The data, measured from ship and low-flying aircraft platforms, also yield the zenith angle dependence of the surface absorption. The clear-sky data are representative of dry regions east of the date line during March 1993.

Likewise, a combination of tropopause albedo measurements from the ER-2 aircraft and Earth Radiation Budget Experiment (ERBE) clear-sky TOA albedos are used to find the absorption of solar radiation by the atmosphere (integrated from the surface to the TOA). Clear-sky TOA albedo is computed from the ER-2 tropopause measurements using a radiative transfer model and measurements of stratospheric aerosol and ozone. The computed TOA albedos agree with ERBE at about 6% for overhead sun. The diurnal average fractional atmospheric column absorption is 20.2% ± 1.6%.

Two multispectral radiation models agree to within 5 W m^{-2} of the observed daily average clear-sky oceanic solar absorption when the atmospheric profile is constrained by measurements and the observed TOA albedo is used as a boundary condition.

1. Introduction

For the past five years, numerous studies (Ohmura and Gilgon 1993; Wild et al. 1995; Ramanathan et al. 1995; Arking 1996) have identified a discrepancy on the order of 10–35 W m^{-2} between diurnally averaged net surface solar radiation measured at the earth's surface and that predicted by radiative transfer models. By noting that the models agree with observations at the top of the atmosphere (TOA), Wild et al. attribute the deficit to an absorption by the atmosphere not present in the models. Whether or not this absorption exists and the extent to which clouds may be responsible has been debated vigorously (Stephens and Tsay 1990; Cess et al. 1995; Pilewskie and Valero 1995; Li et al. 1995; Stephens 1996; Arking 1996). Some observations suggest that a significant fraction (10–30 W m^{-2}) of the missing surface radiation may be due to absorption occurring in the cloud-free atmosphere (Wild et al. 1995; Arking 1996).

We approach the validation of atmospheric absorption of solar radiation under *clear* skies as an important research problem independent of the cloud absorption issue. The purpose of this study is to (a) establish a baseline value for the clear-sky net surface solar radiation at the ocean surface, (b) use TOA and tropopause data to measure how much the cloud-free atmosphere absorbs, and (c) assess how well current state-of-the-art models reproduce these values. Toward this end, we use data from the Central Equatorial Pacific Experiment (CEPEX), conducted from 7 March 1993 to 6 April 1993 (Center for Clouds, Chemistry and Climate 1993). Unique properties of the central equatorial Pacific are that the influences of pollution and continental aerosol are minimal and the concentration of water vapor—the primary solar absorber in the atmosphere—is large. Agreement with models would

Corresponding author address: Mr. William Conant, Center for Clouds, Chemistry and Climate, Scripps Institution of Oceanography, UCSD, 9500 Gilman Drive, Mail Code 0239, La Jolla, CA 92093-0239.
E-mail: billc@fiji.ucsd.edu

TABLE 1. A partial list of symbols.

Symbol	Definition
S^- (S^-_{CS})	Downward surface solar radiation in W m^{-2} (clear-sky)
S^+ (S^+_{CS})	Upward surface solar radiation in W m^{-2} (clear-sky)
S (S_{CS})	Net surface solar radiation (clear-sky)
t (t_{CS})	Atmospheric transmittance (clear-sky)
s (s_{CS})	Surface absorptivity (clear-sky)
S_0	Mean solar constant in W m^{-2}
ε	Correction to S_0 for orbital eccentricity
θ_0	Solar zenith angle
μ_0	Cosine of the solar zenith angle
α^P (α^P_{CS})	TOA albedo (clear-sky)
α^T (α^T_{CS})	Tropopause albedo (clear-sky)
α^S (α^S_{CS})	Surface albedo (clear-sky)
A (A_{CS})	Solar absorption by the atmospheric column in W m^{-2} (clear-sky)
a (a_{CS})	Atmospheric absorptivity (clear-sky)
p	Column precipitable water vapor in kg m^{-2}
$\varepsilon_{Instrument}$	Pyranometer instrumental accuracy
$\sigma_{Variance}$	Variance of surface insolation
$\varepsilon_{VICKERS}$, $\varepsilon_{P\text{-}3}$	Experimental uncertainty of $\langle s_{CS} \rangle$ − platform specific
$\langle\ \rangle$	Average from $\theta_0 = 0°$ to 45°
$[\ ]$	Average from $\theta_0 = 0°$ to 90°

constrain our uncertainty in absorption due to (subsaturated) water vapor and remote oceanic aerosols. The sensitivity of clear-sky solar radiation to changes in the atmospheric profile is small. Therefore, the experimental uncertainty of each measurement and model result must be quantified (and minimized) for a meaningful comparison. We introduce a new method to measure the clear-sky surface global radiation and estimate the experimental uncertainty of this value both as functions of the solar zenith angle. Likewise, we cross-compare measurement techniques and platforms. The model results are validated against the measurements only after the sensitivities of the model results to the range of constraining parameters are ascertained.

The measurements and data analysis are presented in section 2. Two models are briefly described in section 3. Results and conclusions are presented last. For reference, Table 1 includes the symbols used in the paper. A detailed description of the analytical procedures used in this paper have been presented in Conant (1996).

2. Measurements

Expressed as a radiant flux density, the solar energy absorbed by the atmospheric column (A) is the difference between the net TOA solar radiation (P) and the net surface solar radiation (S)

$$A = P - S, \tag{1}$$

where ''net'' denotes the difference between the downward and upward solar radiation—for the TOA and surface, respectively, we have $P = P^- - P^+$ and $S = S^- - S^+$. The insolation (downward solar radiation) at the TOA is the product of S_0, the solar constant for mean Earth–Sun distance; ε, the correction for orbital eccentricity; and μ_0, the cosine of the solar zenith angle. Zenith angle and Earth–Sun distance estimates are obtained using a solar ephemeris (Michalsky 1988; Spencer 1989).

Changes in Earth–Sun distance can complicate using radiant flux densities (units: W m^{-2}) over seasonal time periods, so we normalize the pyranometer measurements by the TOA insolation yielding an atmospheric transmittance ($t = S^-/S_0\varepsilon\mu_0$). For similar reasons, instead of using upward solar radiation, we use albedo, the ratio of upward to downward solar radiation. (In this study, we use measurements of surface, tropopause, and TOA albedo.) Thus, the normalized solar radiation budget yields

$$a = 1 - \alpha^P - s, \tag{2a}$$

where a is the atmospheric absorptivity, α^P is the TOA albedo, and s is the fractional surface absorption (surface absorptivity), which is determined from

$$s = t(1 - \alpha^S), \tag{2b}$$

where α^S is the ocean surface albedo.

Clear-sky values, denoted by the ''CS'' subscript, are strongly dependent on solar zenith angle, (θ_0). Thus for clear skies, the atmospheric and surface absorptivities are represented by

$$a_{CS}(\theta_0) = 1 - s_{CS}(\theta_0) - \alpha^P_{CS}(\theta_0) \tag{3a}$$

and

$$s_{CS}(\theta_0) = t_{CS}(\theta_0)[1 - \alpha^S_{CS}(\theta_0)]. \tag{3b}$$

This section presents our best measurement of the above quantities.

a. Surface absorptivity

1) PYRANOMETER SPECIFICATIONS

Surface insolation (equivalently, downward solar radiation, or global radiation) was measured during CEPEX from the USC Research Vessel *J. Vickers* while cruising on a 2°S track between the Solomon Islands and Christmas Island. An upward facing hemispherical field-of-view cosine-weighted Kipp & Zonen CM 11 pyranometer took measurements at 10-s intervals. The instrument's 95% response time is 15 s. A cardanic gimbal mounting was used to minimize pitch and roll effects, which was located on the front of the uppermost deck of the ship to reduce the influence of the ship's mast. The spectral range of the pyranometer is 0.295–2.8 μm. A relatively transmissive atmospheric band between 2.8 and 4 μm is responsible for an additional 0.6% of the surface insolation under clear skies, which has been accounted for in the calibration procedure at Deutscher Wetterdienst in Hamburg, Germany. The pyranometer has a saturation limit of 1400 W m^{-2}, which was reached on several occasions when nearby reflective clouds enhanced the diffuse sky radiation into the pyranometer while not blocking the direct solar radiation. (This does not concern the authors, as the *clear-sky*

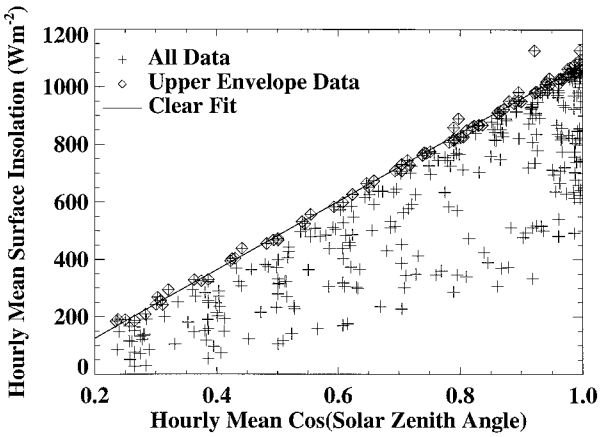

FIG. 1. *Vickers* pyranometer measurements of hourly averaged insolation as a function of the hourly averaged cosine of the solar zenith angle. Data are screened for continuity over a full 1-h period. The data are oversampled so that hourly averages are reported at half-hour intervals to improve clear-sky sampling. The line is an upper envelope linear fit of the form $S_{CS}^{-} = 1193\mu_0 - 113$ (W m^{-2}). The upper envelope fit is determined by iteratively discounting points that fall below 1σ of a least squares linear fit, until the algorithm converges (i.e., a set of points is found for which all points below the fit fall within 1σ of the linear fit to the subset).

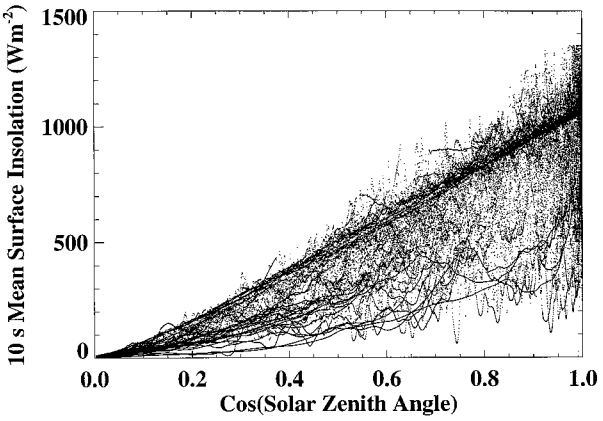

FIG. 2. *Vickers* pyranometer data at the 10-s data rate plotted versus cosine of the solar zenith angle.

insolation at the surface is not expected to exceed $S_0\varepsilon \cong 1384$ W m^{-2}.) The World Meteorological Organization has classified the instrument as a ''secondary standard,'' which allows for an uncertainty in the measurement of daily averaged downward insolation of at most 2%. During pre- and postcruise calibrations at Deutscher Wetterdienst, the pyranometer agreed within 0.5% with respect to a standard radiometer.

2) CLEAR-SKY IDENTIFICATION

Obtaining clear-sky measurements in the central equatorial Pacific is difficult due to the nearly ubiquitous presence of either deep convective or trade cumulus clouds. We consider two independent methods that use the entire pyranometer time series to determine the clear-sky surface insolation (or equivalently, the clear-sky transmittance) as a function of solar zenith angle.

The first method, proposed by Cess et al. (1993), notes that there is a nearly linear relationship between the hourly mean surface insolation and hourly mean cosine of the solar zenith angle, which forms an upper bound on the all-sky (clear + cloudy) data. Following their study, we obtain a linear relationship between S_{CS}^{-} and μ_0 for solar zenith angles less than 75° (Fig. 1). Note from Fig. 1 that that there are several anomalously high values, which correspond to the cases when reflection off the sides of nearby bright clouds increases the diffuse sky radiation without any effect on the direct solar beam. These ''3D'' cloud effects may complicate the accurate estimation of an upper envelope from short period averages. Using longer period averaging to eliminate the 3D effects unfortunately reduces the chance of sampling clear scenes. Also, the upper envelope method does not yield an uncertainty estimate in the clear-sky surface insolation, which will be necessary to interpret the model comparison.

To handle the above issues, we propose a peak frequency density (PFD) method that uses 10-s resolution pyranometer data (Fig. 2) both to account for the 3D cloud effects and to estimate the precision of the clear-sky measurement. To do this, we must first assume that clear skies correspond with the maximum density of measurements apparent in Fig. 2. To understand this assumption, consider the frequency density $\rho(\theta_0, t)$, which is computed as a function of solar zenith angle and atmospheric transmittance. Transmittance is used as the independent variable in lieu of insolation because of seasonal changes in Earth–Sun distance; likewise, solar zenith angle is preferred over μ_0 to better represent the time sampling. The frequency density for three fixed solar zenith angles is illustrated in Fig. 3. For a fixed solar zenith angle, normal changes in a clear-sky atmospheric profile will produce only small changes in atmospheric transmittance, yielding a dense, narrow peak in $\rho(\theta_0, t)$ maximum where $t = t_{CS}(\theta_0)$. In contrast, the smallest variations in a cloud field will produce large changes in the transmission, yielding broader shallower peaks in the frequency density. Even if clear skies occur only rarely, their reproducibility will cause the frequency density to be maximum where the transmission corresponds to clear skies ($t = t_{CS}$). It can be seen from Fig. 3 (at 60°) that the PFD method begins to break down for slant zenith angles due to dispersion of the clear-sky signal. This dispersion is most likely due to enhanced cloud contamination, variability of clear-sky optical depth, and perhaps a shading of the pyranometer during evening hours from the highest parts of the ship's mast. For this reason, we limit our clear-sky measurement (unless otherwise stated) to zenith angles less than 45°.

There is a variance associated with each of the highest peaks in the frequency density function for a given solar zenith angle (see Fig. 3). The standard deviation of each

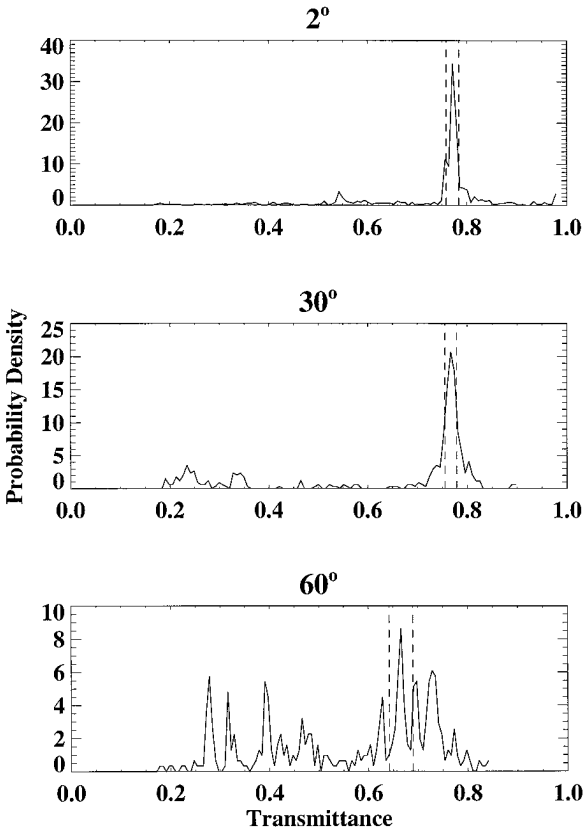

FIG. 3. Histogram of transmittance for three given solar zenith angle ranges: 2°–3°, 30°–31°, and 60°–61°. The frequency density is a relative measure of the number of observations as a function of transmittance. The PFD method assumes clear skies cause the peak in the frequency density; the variance of this peak is shown by the dashed lines. Because of the dispersion apparent at 60°, we limit the use of this method to solar zenith angles less than 45°.

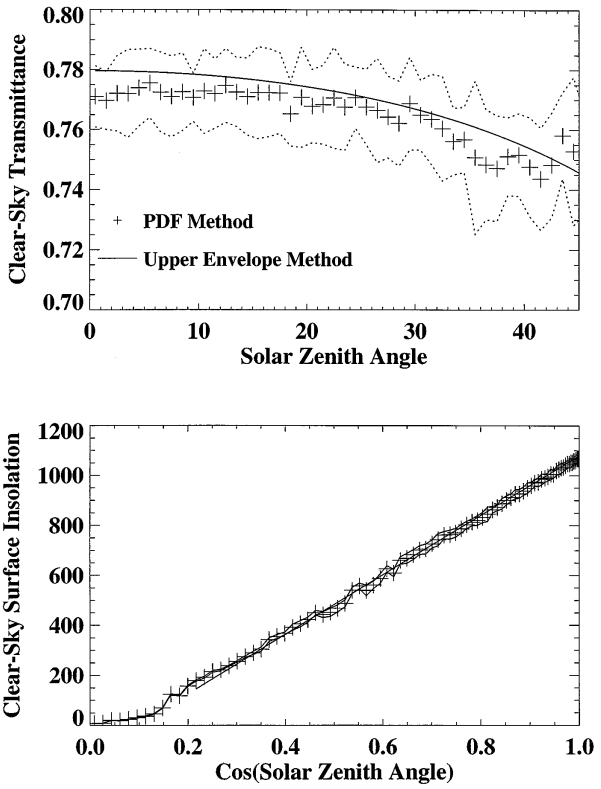

FIG. 4. Results from the PFD clear-sky method. (a) Clear-sky transmittance plotted against solar zenith angle. Each point represents the transmittance that was observed most often at each zenith angle. Error bars are included that represent the standard deviation of the signal. The sensitivity in t is roughly 0.007. For comparison, the curve represents the clear-sky transmittance calculated from the Cess et al. method (Fig. 1). (b) Same as (a) except clear-sky insolation is plotted vs μ_0 for the full range of zenith angles for comparison with Figs. 1 and 2. Compared to the Cess et al. linear fit, the PFD method has a mean bias of 1% (+3 W m^{-2} in the daily average sense) and a root-mean-square deviation of 13 W m^{-2}.

peak, outlined in Fig. 3, is taken to be the precision of the clear-sky measurement.

The PFD method will not work if there are no clear scenes during the period. Errors in the PFD method are likely to arise if the following situations are far more prevalent than clear skies: (a) the cloud field includes uniform thin cirrus, which will reduce the surface radiation without having the variability characteristic of other cloud fields; or (b) the field includes broken trade cumulus, which would often enhance diffuse sky radiation into the pyranometer enough to skew the clear-sky signal toward the high-transmittance side, causing an overestimation of t_{CS}. We assume these potential errors are encompassed within the standard deviations shown in Fig. 3.

The PFD method yields the clear-sky transmittance, $t_{CS}(\theta_0)$, from 0° to 45° solar zenith angle at 1° resolution in solar zenith angle (Fig. 4a). For comparison with Fig. 1 and 2, the clear-sky surface insolation, $S_{CS}^{-}(\mu_0)$, is shown for the full range of zenith angles (Fig. 4b). The PFD method shows excellent agreement with the Cess et al. (1993) upper envelope method within the stated variance.

3) SURFACE ALBEDO AND NET SURFACE SOLAR RADIATION

Next we obtain the net surface solar radiation, or equivalently the surface absorptivity, using (3b) with the clear-sky transmittance determined above and CEPEX measurements of clear-sky surface albedo. The *Vickers* made no measurement of surface albedo. The NOAA P-3 aircraft, which flew during CEPEX at altitudes as low as 30 m, carried both upward and downward facing pyranometers, although the observed range of solar zenith angles is limited. Thus, we compare the P-3 clear-sky surface albedo described in Collins et al. (1996) with results from Briegleb et al. (1986), who parameterize ocean surface albedo both for direct solar and diffuse sky radiation based on observations. The discrete ordinate code described in section 3b is used to find the ratio of diffuse to direct radiation at the ocean surface under clear skies and from this, a model albedo is computed as a function of solar zenith angle. The P-3 observations exceed the Briegleb model by 0.0015 with

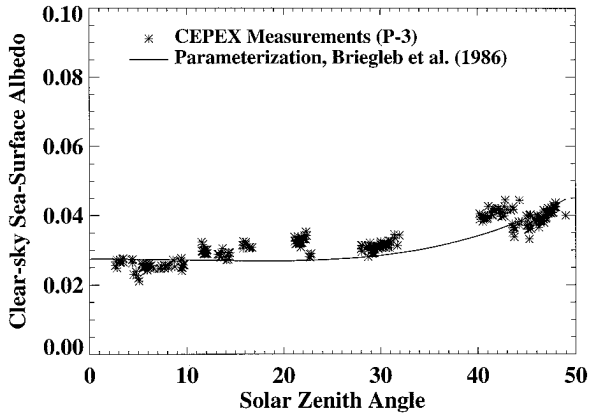

FIG. 5. Clear-sky surface albedo estimated from Briegleb et al. (1986) plotted with observations from the P-3 aircraft, flying at 30–100 m altitude. The (flux-weighted) mean bias is 0.0015 and the variance is 0.0035.

a variance of 0.0035 (Fig. 5). This bias in the aircraft albedo is expected because of aerosol and Rayleigh scattering occurring in the 30–100 m between the dark ocean surface and the aircraft. (In contrast, a highly absorbing medium over a brighter surface could yield an albedo that decreased with altitude.)

Given the surface absorptivity obtained from (3b), we construct a representative average. Lacking robust clear-sky data for solar zenith angles greater than 45°, our best average for comparison with the models will be a midday average from 0° to 45° solar zenith angle. (In what follows, we represent the 0° to 45° average by the symbol $\langle\ \rangle$ and the 0° to 90° solar zenith angle average, that is, an equatorial equinox diurnal average, by the symbol [ ].) For the *Vickers*, $\langle s_{CS}\rangle_{VICKERS} = 0.744$. Pyranometer measurements taken from P-3 are analyzed in an identical manner and agree well with the *Vickers* measurements at $\langle s_{CS}\rangle_{P\text{-}3} = 0.746$. Most of this discrepancy can be explained by absorption occurring between the aircraft and the surface.

4) EXPERIMENTAL UNCERTAINTY

The experimental uncertainty of our mean surface absorptivity is computed based on the 2% instrumental accuracy (for daily mean values) and the averaging uncertainty due to a limited sample size. A normal distribution for uncorrelated errors is assumed, and thus the experimental uncertainty based on the *Vickers* data ($\varepsilon_{VICKERS}$) is given by

$$(\varepsilon_{VICKERS})^2 = (\varepsilon_{instrument})^2 + (\sigma_{Variance})^2/N. \qquad (4)$$

Here, $\varepsilon_{instrument}$, the instrumental accuracy, equals 0.015 (2% of $\langle s_{CS}\rangle$). The second term on the right side of (4) is the square of the signal variance, $(\sigma_{Variance})^2$, divided by N, the number of *independent* samples provided by the measurements. The flux-weighted variance ($\sigma_{Variance}$), which was obtained from the PFD method, is 0.014.

TABLE 2. The estimates used to determine the experimental uncertainty in the 0°–45° average of surface absorptivity.

	Fractional surface absorption	Experimental uncertainty	Instrumental accuracy	Clear-sky variance	Number ind. samples
Vickers	0.744	±0.016	0.015	0.014	6
P-3	0.746*	±0.020	0.016	0.012	1
Combined	0.744	±0.010	—	—	—

* The P-3 measurement includes absorption from the lowest 30–100 m of the atmosphere.

This arises from changes in aerosol optical depth and column precipitable water. The small (<1 W m^{-2}) precision (i.e., sensitivity and reproducibility) of the pyranometer is neglected. The variance estimate may be large due to cloud contamination. It is cautioned that $\sigma_{Variance}$ is determined by observations spanning a 2-week period and does not necessarily reflect the climatological variability in the clear-sky surface radiation. It is not possible to take each day of clear-sky observations as an independent measurement because not even one day was entirely clear. However, on the 11-day cruise between the Solomon Islands and Christmas Island, the *Vickers* observed more than 36 h of observations within clear-sky limits ($s_{CS} \pm \sigma_{Variance}$ for $\theta_0 < 45°$). At equatorial latitudes during March, the sun spends almost exactly 6 h day^{-1} within the zenith angle range 0°–45°. Thus, the 36 h of clear-sky measurements are divided into six independent 6-h periods to obtain $N = 6$ and $\varepsilon_{VICKERS} = 0.016$ from (4).

The use of two platforms (e.g., *Vickers* and P-3) that agree on the surface measurement should increase our confidence in the average value. We repeat the uncertainty analysis for the P-3 pyranometer data, which is summarized with the *Vickers* in Table 2. Assuming that the errors associated with the uncertainties in the *Vickers* and the P-3 measurements are independent and normally distributed, the relation should hold that

$$(\varepsilon_{TOTAL})^{-1} = (\varepsilon_{VICKERS})^{-1} + (\varepsilon_{P\text{-}3})^{-1}. \qquad (5)$$

Following this method, $\varepsilon_{TOTAL} = 0.009$, which we round up to 0.010. Our final estimate of $\langle s_{CS}\rangle$ is thus 0.744 ± 0.010.

b. TOA albedo and atmospheric absorptivity

Having estimated the surface absorptivity, our next objective is to estimate the atmospheric absorptivity. For this purpose, we require TOA albedos. CEPEX measured tropopause albedos from the high-altitude ER-2 aircraft and we use a radiation model to convert the tropopause albedos to TOA albedos by accounting for the stratospheric effects, that is, ozone and other gaseous absorption, and stratospheric aerosols. We must, however, address one important sampling problem with the ER-2 tropopause albedos. They did not cover the exact

time, location, or field of view as the surface ship measurements. Therefore, we need an understanding of the spatial and temporal variability of the clear-sky albedos over the central equatorial Pacific. We resort to the pixel level ERBE TOA albedo data for March 1985 to 1989 (the period for which ERBE data are available) to better understand the sampling issue.

The NASA ER-2 flew at 18 km, measuring upward and downward solar radiation with broad spectral range hemispheric field-of-view solar radiometers accurate to 1 W m^{-2}. A partial clear-sky screening using nadir infrared radiances is provided by Collins et al. (1996). Because the downward facing instrument is hemispheric and the screening is at nadir, the data may be contaminated by clouds at side viewing angles. Collins et al. provide a solar zenith angle dependent clear-sky albedo based on the lowest of the ER-2 measurements.

The ER-2 tropopause albedo measurements (α^T_{CS}) are converted to a TOA albedo (α^P_{CS}) using the Disort-MS radiative transfer model. As will be seen shortly, the conversion factor is small. A thin stratospheric aerosol residual from the Pinatubo eruption in 1991 was measured by a Total Direct-Diffuse Multichannel Radiometer (TDDR) aboard the ER-2 by a method described in Valero and Pilewskie (1992). This radiometer separately measures direct beam radiation and diffuse sky radiation using a shadowing method. Based on these spectral data, a model stratospheric aerosol of optical depth 0.05 (shortwave of 1.0 μm), asymmetry parameter 0.71, and single-scattering albedo 0.997 is included in a radiative transfer model (section 3b) as a 1-km thick layer immediately above the aircraft. The model also includes an ozone profile from *Vickers* balloon soundings. The ratio $\alpha^P_{CS}/\alpha^T_{CS}$ is computed for clear skies as a function of solar zenith angle. The measured tropopause albedo is then multiplied times the model ratio to get a corresponding estimate of the TOA albedo. The ratio $\alpha^P_{CS}/\alpha^T_{CS}$ is 1.034 $\pm$ 0.004 over the range $\theta_0 = \{0°–45°\}$ and thus has a small effect on the estimated TOA albedo. (If the Pinatubo aerosol were not present in the model, the ratio would be nearly unity due to the competing physics of ozone absorption and scattering by the thin background stratospheric aerosol.)

Clear-sky March ERBE pixel data from 1985 through 1989 are used for estimating the variability of the clear-sky TOA albedos. The *Earth Radiation Budget Satellite* (*ERBS*) was not in a sun-synchronous orbit, so albedo is sampled for all solar zenith angles. The clear-sky screening simultaneously considers infrared and visible criteria, allowing for a cloud fraction of up to 5%. Thus, the mean albedo may be slightly large (Ramanathan et al. 1989).

To compare the ERBE data (which was not affected by the Pinatubo aerosol) to the CEPEX data, model computations are performed with and without the Pinatubo aerosol. The TOA albedo is higher by a factor of about 1.03 in the presence of the Pinatubo aerosol when compared to a similar atmosphere with only a background

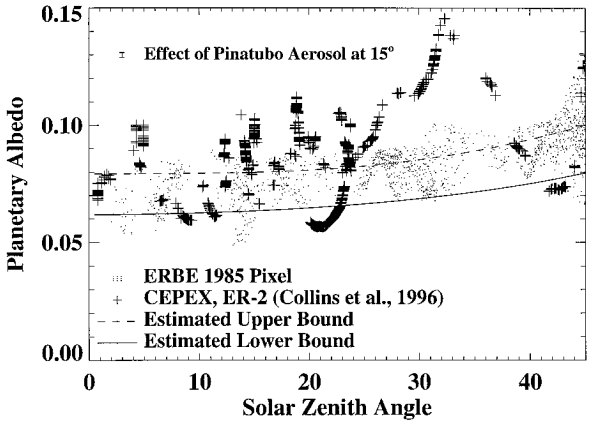

FIG. 6. Clear-sky TOA albedo: The + marks indicate ER-2 broadband albedo measurements from the tropopause, corrected to reflect TOA albedos. They have been screened for clear sky by separate, nadir viewing instruments. The points are ERBE pixel data for the central Pacific (0°–5°S; 165°E–165°W) from March 1985, corrected to simulate the presence of the stratospheric aerosol observed during 1993. The magnitude of the corrections is shown as a range bar. Two lines are shown that represent our upper and lower estimates of clear-sky albedo. The upper estimate is taken from the ERBE March 1986 gridded mean albedo (the highest of the five ERBE years), and the lower estimate is taken from Collins et al. (1996). (There are still data below the lower estimate to allow for natural variability.)

stratospheric aerosol. Using this factor, the ERBE TOA data used for comparison with CEPEX tropopause and surface data are corrected to include the Pinatubo effect.

The CEPEX TOA albedos inferred from ER-2 and ERBE measurements are shown in Fig. 6. The variability for both the ER-2 and the ERBE pixel measurements is due to a combination of cloud contamination effects and changing atmospheric aerosol and surface sea state. (Water vapor variability has a small direct effect on the clear-sky TOA albedo due to a lack of scattering in the near-infrared.) It is reassuring that the lowest albedos inferred by ERBE are corroborated by the ER-2 measurements, for the lowest albedos are the least likely to be affected by cloud contamination.

For an accurate measurement of atmospheric absorptivity, we must choose a clear-sky TOA albedo that is consistent with the PFD clear-sky screening at the surface. If more cloud contamination is allowed at the TOA than at the surface, the TOA reflectivity will be overestimated, and thus the atmospheric absorption will be underestimated. With no independent way of separating the natural variability of clear-sky TOA albedo from the cloud effects, we must consider a wide but reasonable range of clear-sky albedos. We choose an upper and lower bound TOA albedo based on the ER-2 and ERBE data presented in Fig. 6. As the upper bound, we take the ERBE March 1986 gridded mean albedo which is 0.080 for overhead sun. 1986 is chosen because it showed the largest mean clear-sky albedo from the five Marches during ERBE (1985–89); the lowest ERBE mean March albedo (from 1985) is 0.074 for overhead sun. As a lower bound, we take the zenith-angle-dependent clear-sky

TOA albedo from Collins et al. (1996), which, after being enhanced by the Pinatubo aerosol, has a 0.062 albedo for overhead sun. This lower bound is chosen because it is consistent with the lowest albedos from both the ER-2 and the ERBE pixel measurements.

Now we are ready to estimate the atmospheric absorption under clear skies using (3a). The 0°–45° flux-weighted averages are represented by $\langle \alpha^P_{\rm CS} \rangle$ for the TOA albedo and $\langle a_{\rm CS} \rangle$ for the atmospheric absorptivity. The experimental uncertainty in the computed atmospheric absorption is taken to be the root mean square (rms) of the uncertainty at the surface and at the TOA.

CEPEX data in conjunction with ERBE yield the following estimates:

$$\langle s_{\rm CS} \rangle = 0.744 \pm 0.010$$

$$\langle \alpha^P_{\rm CS} \rangle = 0.076 \pm 0.009$$

$$\langle a_{\rm CS} \rangle = 0.180 \pm 0.013.$$

These estimates are restricted to 0°–45° because the uncertainty introduced by the clear-sky identification scheme becomes larger for zenith angles greater than 45°. They are representative of relatively dry (column precipitable water vapor $\sim$ 40 kg m^{-2}) tropical regions east of the date line. In section 3c, the model results are used with the CEPEX observations to extrapolate both daily average and climatological baseline values for the above quantities.

3. Model validation

In this section, we examine how well two state-of-the-art models reproduce the surface and atmospheric absorptivities measured in the previous section. The first model is the Li et al. (1993a) transfer function; the second is a 38-spectral-band discrete ordinates radiative transfer model. Clear-sky model radiative fluxes are most sensitive to solar zenith angle, surface albedo, and the atmospheric profiles of humidity, ozone, and aerosol. CEPEX observations provide all but the aerosol profile. We tune the unmeasured aerosol effect by applying the measurement of TOA albedo as an additional constraint on the models. The models will be judged on their ability to partition solar absorption between the atmosphere and the ocean consistently with the observations. This partitioning is particularly sensitive to atmospheric absorption by ozone, aerosols, and water vapor.

a. The modified Li et al. transfer function (MLTF)

The Li et al. (1993a) transfer function attempts to derive surface radiation solely from TOA satellite measurements. It was suggested that there is a linear relationship between TOA reflected solar radiation and net surface solar radiation; however, this relationship was found to be sensitive to both cloud optical depth and surface albedo (Cess et al. 1991). Li et al. find a linearity *insensitive* to cloud optical depth and surface albedo if solar zenith angle and column precipitable water vapor (p) are explicitly included as independent variables in the relationship. They propose

$$s = A(\mu_0, p) - B(\mu_0, p)\alpha^P, \tag{6}$$

where $A(\mu_0, p)$ and $B(\mu_0, p)$ are offset and slope terms derived from radiative transfer model results. When compared against a limited sample of both clear and cloudy surface measurements, the transfer function has proven accurate with a bias of less than 2 W m^{-2} (Li et al. 1993b). While sensitive to water vapor variations, the Li et al. transfer function (LTF) was derived using a fixed subarctic summer atmosphere and an Arctic haze aerosol of 0.05 optical depth. The ozone and aerosol profiles included in the parameterization are highly absorptive and thus should introduce a bias if we apply it to the equatorial Pacific. Before using the LTF model, we correct for the ozone bias. Calculations from the radiative transfer model presented in section 3b show that increasing the ozone from that observed during CEPEX to a subarctic summer profile introduces a 0.006 bias in the atmospheric absorptivity (0°–45° average), resulting in an underprediction of the surface absorptivity. The corrected model is termed the ''Modified Li et al. Transfer Function'' (MLTF). A second bias may be present due to the highly absorptive Arctic haze aerosol in the LTF model. We will retain this bias in the MLTF model to illustrate the sensitivity of atmospheric absorption to differing aerosol types.

As input to (6), we take CEPEX precipitable water measurements and clear-sky TOA albedos to estimate the clear-sky surface absorptivity as a function of solar zenith angle. Measurements of column precipitable water vapor are taken from Vaisala radiosondes that were launched at 6-h intervals during the entire *Vickers* cruise (Weaver et al. 1994). These instruments are accurate to 10% in relative humidity, 1°C in temperature, and 1 mb in pressure. The temperature and pressure sensors were calibrated against ship measurements before each launch. From these vertical profiles, a specific humidity is computed and then integrated from the surface to above the tropopause to obtain a column precipitable water content (p). We assume that the error in this measurement from the instrument accuracy, altitude range, and integration resolution is within 10%. The *Vickers* was under a region of suppressed convection and encountered a majority of clear-sky scenes while on an eastward course along 2°S east of the date line. These dry soundings are averaged to get $p = 42$ kg m^{-2}, which is used as input to the transfer function.

The MLTF model predicts the surface absorptivity under clear skies to be 0.733 ± 0.009 (0°–45° average), and the atmospheric absorptivity is 0.191 ± 0.001. These have experimental uncertainties that result from the experimental uncertainty of the TOA albedo used in the model. The low TOA albedo limit (case 1) yields a higher surface absorptivity than the high albedo limit (case 2). Because the MLTF model increases scattering

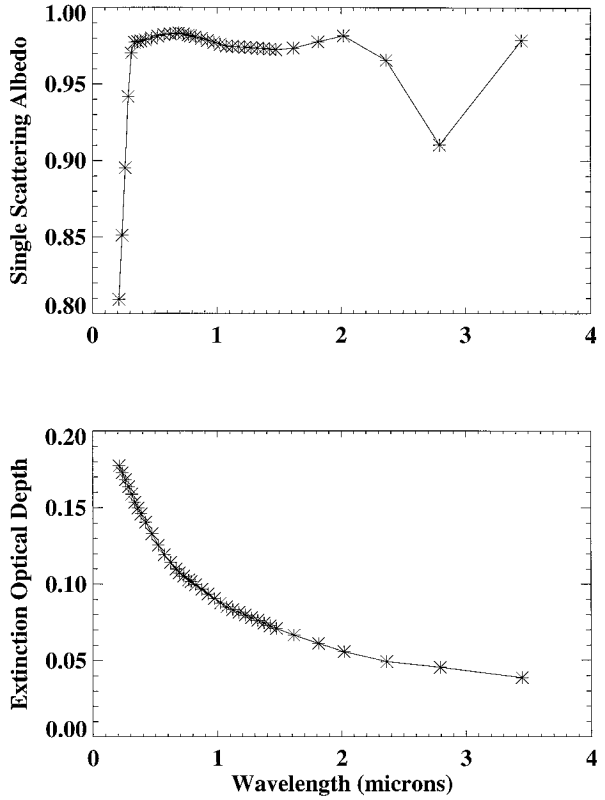

FIG. 7. The LOWTRAN 7 maritime boundary layer aerosol scheme used to compute the single-scattering albedo and aerosol optical depth for a maritime aerosol of visibility 27 km. The optical depth has been tuned in the discrete ordinate model so the TOA boundary matches the median TOA albedo case. Model runs with this aerosol compare well with those using the Coakley et al. (1983) parameterization for a marine aerosol of a comparable optical depth. Both schemes are based on Shettle and Fenn (1979) tabulated aerosol properties. (The LOWTRAN 7 aerosol has a small continental component, accounting for some absorption.)

to determine the relationship between surface absorptivity and TOA albedo, the atmospheric absorption changes little between the two cases. To avoid a ''wet bias,'' where mean water vapor is used with the clear-sky albedos characteristic of more dry scenes, we have specifically chosen a dry atmosphere from the suppressed convection regions under which tropical clear skies are found. If the climatological water vapor of 50 kg m^{-2} were used, the predicted atmospheric absorptivity would be increased by 0.011.

b. Multispectral discrete ordinate code (Disort-MS)

The second model, Disort-MS, developed by Shi (1994), is based on a multispectral implementation of Stamnes et al.'s (1988) discrete ordinate radiative transfer algorithm using 32 layers, four streams, 38 spectral bands, a Lambertian surface boundary condition, and gas optical depths determined from an exponential sum-fitting technique. Profiles of temperature, ozone, and water vapor are taken from CEPEX soundings; a climatological carbon dioxide mixing ratio for 1993 is used. As in the MLTF model, the water vapor profile is an average taken from regions of suppressed convection. The ozone profiles are taken from the same domain as the water vapor soundings. The volcanic aerosol measured by the ER-2 TDDR is placed as a 1-km-thick layer above 18 km. For lack of boundary layer aerosol measurements, we have included a boundary layer aerosol profile whose optical properties are given by the LOWTRAN 7 maritime aerosol parameterization developed primarily from observations reported by Shettle and Fenn (1979). The optical depth of the aerosol is scaled to achieve consistency with the range of measured 0°–45° average TOA albedos. The aerosol single-scattering albedo and optical depth is plotted in Figs. 7a,b for the median TOA albedo case. The model uses the solar zenith-angle-dependent surface albedo described above.

TABLE 3. The 0°–45° average values of surface absorptivity, atmospheric absorptivity, and TOA albedo from observations, the Disort-MS model, and the MLTF model. The 0°–45° average provides the most accurate measurement of clear-sky solar radiation. For the observations, the ranges are derived from the experimental uncertainty of the measurements. For the models, uncertainties are derived from the model sensitivity to the TOA albedo, used as a boundary condition.

	Observations	Modified Li et al.	Disort-MS
$\langle s_{CS} \rangle$	0.744 ± 0.010	0.733 ± 0.009	0.741 ± 0.012
$\langle \alpha^P_{CS} \rangle$	0.076 ± 0.009	0.076 ± 0.009	0.076 ± 0.009
$\langle a_{CS} \rangle$	0.180 ± 0.013	0.191 ± 0.001	0.184 ± 0.003

The 0°–45° average surface absorptivity for Disort-MS is much higher than for the MLTF model at 0.741 ± 0.012, and the atmospheric absorptivity is lower at 0.184 ± 0.003. (As with the MLTF model, the experimental uncertainty of the Disort-MS results are tied to the uncertainty of the TOA boundary condition.) The atmosphere is less absorptive in Disort-MS, in part, because the maritime aerosol is less absorptive than the Arctic haze present in the MLTF model. To achieve consistency with case 1, the low albedo case, the boundary layer aerosol optical depth at $\lambda = 0.55$ μm (τ_{BL}) was tuned to 0.03. For case 2, the upper bound albedo case, $\tau_{BL} = 0.24$.

c. Comparison with observations

Table 3 summarizes the observational and model results for the 0°–45° solar zenith angle average of surface absorptivity, atmospheric absorptivity, and TOA albedo. The experimental uncertainty determined for each of the observations is included. Observations agree better with the Disort-MS model than with the MLTF model. This is expected because of the absorptive Arctic haze aerosol in the MLTF model, compared to the maritime aerosol in Disort-MS. The ranges of experimental uncertainty overlap between the three cases (Observed, MLTF, and Disort-MS). We will explore later varying assumptions about the accuracy of our TOA albedo estimate.

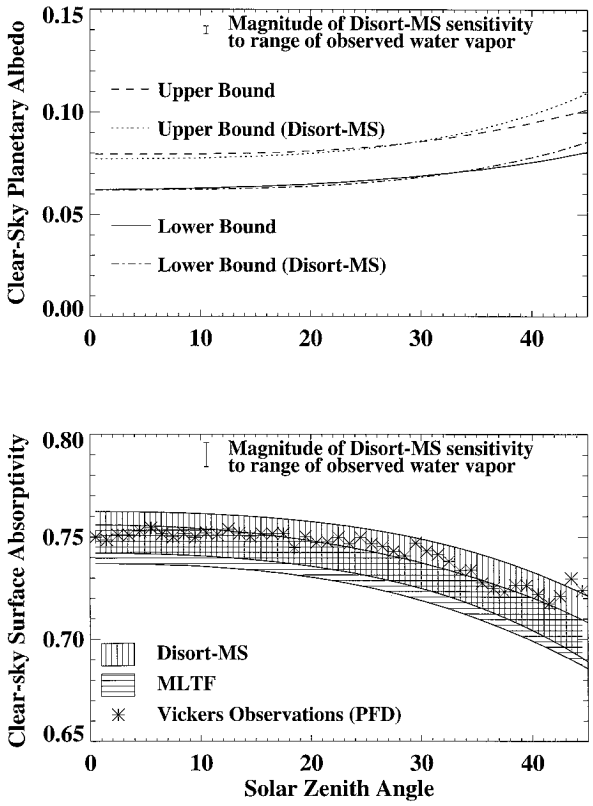

FIG. 8. Comparison between observations and model runs. (a) TOA albedo results from the Disort-MS model are compared to the clear-sky albedo fits. The solid and dashed lines are the same as in Fig. 6, representing the upper and lower bounds from the observations. The dotted line is the low aerosol Disort-MS run, and the dot–dash line is the high aerosol case. The mean water vapor used as input to the model runs is an average over drier regions of the cruise east of the date line. A bar is shown to illustrate the rms model sensitivity (at $\theta_0 = 15°$) to the full range of observed column water vapor from the *Vickers*'s 11-day cruise from Honiara to Christmas Island. (b) Surface absorptivity computed by the two models (Disort-MS, MLTF) for the full range of constraining TOA albedos shown in Fig. 8a. The + symbols are the ship observations from the PFD method. The range bar shows the effect of varying water vapor at constant albedo based on the Disort-MS model.

The model-to-observation comparison is more illustrative as a function of solar zenith angle (Figs. 8a,b). For both models, the surface absorptivity agrees within the stated uncertainty (Fig. 8b). To illustrate the effect of water vapor on the surface absorptivity, the model results were recomputed using profiles from each individual Vaisala sounding during the cruise, including the moist, convectively active regions in the western Pacific where clear skies were rare, at best. The rms variability from such water vapor changes is shown as range bars in Figs. 8a,b. Note from Table 3 and Fig. 8a that the variation of TOA albedo with solar zenith angle differs between the observations and the Disort-MS model (perhaps due to the Lambertian surface boundary condition); regardless, the 0°–45° Disort-MS average albedo has been constrained to match the observations.

TABLE 4. The diurnal (0°–90°) average of CEPEX surface and atmospheric absorption. The observed surface fluxes have been extrapolated from the 0°–45° fractional results (Table 3) and the MLTF diurnal flux.

	Observations	Modified Li et al.	Disort-MS*
$[S_{CS}]$	311 ± 5	307 ± 5	310 ± 7
$[P^{+}_{CS}]$	41 ± 4.5	41 ± 4.5	44.5* ± 5.5
$[A_{CS}]$	89 ± 7	93 ± 0.5	86.5 ± 1.5
$[s_{CS}]$	0.705 ± 0.012	0.696 ± 0.011	0.703 ± 0.016
$[\alpha^{P}_{CS}]$	0.093 ± 0.010	0.093 ± 0.010	0.101* ± 0.012
$[a_{CS}]$	0.202 ± 0.016	0.211 ± 0.001	0.196 ± 0.004

* Note that the Disort-MS column in Table 3 is not constrained to match the observations at the TOA. This is due to a solar zenith angle response in the Disort-MS that is inconsistent with the ERBE observations. This is most likely due to a simplified treatment of the surface albedo in Disort-MS, and the values are only shown for illustrative purposes.

Using absorptivities averaged from 0° to 45° has been useful to analyze data from uncoordinated, moving platforms. However, the results are more easily understood when expressed as diurnally averaged flux densities. The diurnal average will be difficult to obtain because the limitation of the PFD method was to identify clear skies only for zenith angles less than 45°. For lack of a diurnal net surface solar radiation measurement, we extrapolate the value. The extrapolated ''measured'' diurnal net surface solar radiation will be the 0°–45° measurement times the proportionality that relates the diurnal model value to the 0°–45° model value

$$[S_{CS}\ \text{(extrapolated)}] = \langle s_{CS}\ \text{(observed)}\rangle \{[S_{CS}\ \text{(model)}]/\langle s_{CS}\ \text{(model)}\rangle\}. \quad (7)$$

Recall that square brackets indicate a diurnal average, and angle brackets indicate a 0°–45° average. We caution that the Disort-MS model is inappropriate for this use because the *daily averaged* radiative exitance is 2.5–4.5 W m^{-2} higher when compared to the observations (see Fig. 8a). Thus, we use the MLTF model with the 0°–45° surface observations to estimate the observed diurnal flux. With (7), we compute a net surface solar radiation of 311 W m^{-2} (which is remarkably close to the 312 W m^{-2} value calculated when extending the PFD method out to 90°). The uncertainty in the 0°–45° average surface absorptivity translates to a 4 W m^{-2} uncertainty in the diurnal average, which we increase to 5 W m^{-2} because the integration is extrapolated from models. Taking the rms of the uncertainty in net surface solar radiation and the net TOA solar radiation, we have an experimental uncertainty in the diurnal average atmospheric absorption of 7 W m^{-2}. These results are summarized in Table 4. On a diurnal average, the MLTF model has an atmosphere that is 6.5 W m^{-2} more absorptive than the Disort-MS model. Both models agree with observations within the 7 W m^{-2} measurement uncertainty.

In a previous publication by Ramanathan et al. (1995), we computed a net surface solar radiation based on *Vickers* pyranometer measurements of 306 W m^{-2}

in contrast to the 311 W m^{-2} published here. The change of 5 W m^{-2} presented in this paper does not affect the results of the previous study, which explicitly used ERBE albedos with the MLTF model to determine clear-sky surface radiation. In the present study, we use an improved estimate of surface albedo described above, which has been validated by P-3 aircraft measurements. The previous study used a surface albedo presented in Briegleb and Ramanathan (1982), which, at overhead sun, is 1.4% more reflective than the albedo used here. The differences between the two parameterizations are described in Briegleb et al. (1986).

Last, we wish to establish baseline estimates from the CEPEX observations. There are two issues: (i) the measurements presented here are influenced by the presence of the Pinatubo stratospheric aerosol, which should not be included in a climatological baseline estimate; (ii) CEPEX measurements were taken only for a single March, and thus the baseline estimate must include an uncertainty due to interannual variability. The effect of the Pinatubo aerosol is to enhance the TOA albedo by 0.004 on the daily average and likewise reduce the surface absorption (the effect on the atmospheric absorption is small). Also, during the ERBE period, the average clear-sky albedo was observed to vary from the 5-yr mean by only 0.003. Thus, we will take the observed CEPEX values, modify the mean by removing the effect of the Pinatubo aerosol, and increase the stated experimental uncertainty based on the (uncorrelated) ± 0.003 interannual variability observed at the TOA. These result in a baseline March surface absorptivity [s_{CS}] of 0.709 $\pm$ 0.013. The estimate of atmospheric absorptivity remains unchanged at [a_{CS}] = 0.202 $\pm$ 0.016, and the baseline TOA albedo becomes 0.089 $\pm$ 0.010.

4. Summary and conclusions

In summary:

- A peak frequency density method for clear-sky identification is relatively consistent (within 1%) with the linear fit method for determining the clear-sky net surface solar radiation as a function of solar zenith angle, while more accurately accounting for 3D cloud effects at low zenith angles.
- The CEPEX Equatorial Pacific surface absorption was 311 $\pm$ 5 W m^{-2}, or 0.705 $\pm$ 0.012 expressed as a fraction of the TOA insolation. Accounting for the Pinatubo aerosol and interannual variability, we compute a climatological baseline surface absorptivity estimate [s_{CS}] 0.709 $\pm$ 0.013.
- The equatorial clear-sky atmosphere absorbs 89 $\pm$ 7 W m^{-2} or fractionally, 0.202 $\pm$ 0.016 of the diurnally averaged insolation.
- These values correspond to a relatively dry tropical atmosphere with a measured column precipitable water content near 42 kg m^{-2}. We caution that there may be differing cloud screening between the TOA and the surface, which is addressed last.

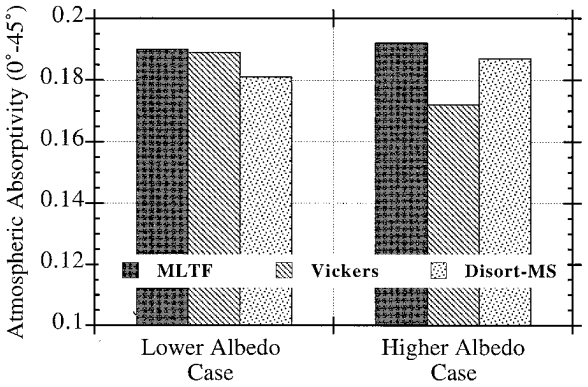

FIG. 9. Atmospheric absorptivity (0°–45° zenith angle average) is computed using the three methods for finding surface radiation (MLTF model, observations, and Disort-MS model) using each of the lower and upper bounds on clear-sky planetary albedo. These are the two extreme albedo estimates; the median case is summarized in Table 3.

- ER-2 lower envelope tropopause albedo measurements corroborate the lowest albedos estimated from ERBE satellite radiances; this both raises the confidence in the ERBE data over the tropical pacific and constrains the monthly average clear-sky albedo during CEPEX to 0.093 $\pm$ 0.010.
- When constrained to reproduce measured clear-sky TOA albedos, current state-of-the-art radiative transfer models predict the clear-sky net surface solar radiation well within the experimental uncertainty of the measurement ($\pm$5 W m^{-2} diurnally averaged).

We would like to conclude with an important issue regarding atmospheric absorption, the question being: ''Is there an unexplained absorption in the clear-sky atmosphere that contributes to that observed for mean conditions?'' From the data presented in Tables 3 and 4, which include a large uncertainty at the TOA, the absorption is well within the experimental uncertainty. However, it may be that our fundamental uncertainty in the clear-sky albedo is due to cloud contamination, which will only decrease, not enhance, our estimate of the column absorbed solar radiation. To understand the possible effect of cloud contamination on our study, we separately consider the lower and upper range of the clear-sky albedos determined in section 2b.

Figure 9 illustrates the differences in computed atmospheric absorptivites, (0°–45° average) when using each extreme of the clear-sky albedo with the three methods for determining surface radiation (MLTF, observations, and Disort-MS). The atmospheres in the two models are prescribed, so their absorptivity does not change much as TOA albedo is changed. Note that the atmosphere of the MLTF parameterization is 0.007 more absorptive than the conservative aerosol case due, in part, to the absorptive Arctic haze aerosol.

In contrast to the models, the estimate of atmospheric absorptivity from observations is very sensitive to specification of TOA albedo, simply because surface ab-

sorption is constrained. From Fig. 9, if we adopt the higher TOA albedo case, the resulting observed atmospheric absorptivity is inconsistent with either model atmosphere. Adopting the median albedo (not shown in Fig. 9) leads to consistency with the Disort-MS model, but not the MLTF model (see Tables 3 and 4). We note here that the ERBE monthly mean gridded TOA albedo is most consistent with the median and uppermost albedo cases chosen above. Thus, using ERBE albedos with our surface observations leads to best agreement with a nonabsorbing aerosol in the model atmosphere. In contrast, the lower albedo case from Fig. 9 gives results consistent with the MLTF model. Because the MLTF model contains an Arctic haze aerosol more absorptive than the conservative aerosol thought to be present in the Tropics, if we were to assume that the ERBE clear sky is too large (due to cloud contamination or other factors) and adopt the lower albedo case, we would thus be led to conclude there is an unexplained absorption in the clear-sky tropical atmosphere. Even still, the (diurnal average) unexplained absorption represented by this extreme scenario is only on the order of 5 W m^{-2}—within the uncertainty of the surface measurement. Hence, we conclude that the 10–30 W m^{-2} clear-sky model-observations discrepancy found by other studies (Wild et al. 1995; Arking 1996) does not exist in the central equatorial Pacific.

Acknowledgments. This work was supported by NSF Science and Technology Center for Clouds, Chemistry and Climate (C^4) Grant ATM9405024 and DOE-ARM Grant DE-FG03-91ER61198. CEPEX was funded by NSF and DOE. We thank L. Shi for the use of her multispectral implementation of the discrete ordinate code, J. Coakley for his insightful comments regarding the PFD method, and W. Collins for advice regarding the interpretation of his clear-sky analyses. This is C^4 Publication Number 147.

REFERENCES

Arking, A., 1996: Absorption of solar energy in the atmosphere: Discrepancy between model and observations. *Science,* **273,** 779–782.

Briegleb, B., and V. Ramanathan, 1982: Spectral and diurnal variations in clear sky planetary albedo. *J. Appl. Meteor.,* **21,** 1160–1171.

——, P. Minnis, V. Ramanathan, and E. Harrison, 1986: Comparison of regional clear-sky albedos inferred from satellite observations and model computations. *J. Climate Appl. Meteor.,* **25,** 214–226.

Center for Clouds, Chemistry and Climate, 1993: CEPEX experiment design. R. Dirks, R. Grossman, A. Heymsfield, J. Kuettner, V. Ramanathan, and F. Valero, Eds., 56 pp. [Available from Center for Clouds, Chemistry and Climate, Scripps Institution of Oceanography, University of California, San Diego, CA 92093-0239.]

Cess, R. D., E. G. Dutton, J. J. DeLuisi, and F. Jiang, 1991: Determining surface solar absorption from broadband satellite measurements for clear skies: Comparison with surface measurements. *J. Climate,* **4,** 236–247

——, S. Nemesure, E. G. Dutton, J. J. DeLuisi, G. L. Potter, and J.-J. Morcrette, 1993: The impact of clouds on the shortwave radiation budget of the surface-atmosphere system: Interfacing measurements and models. *J. Climate,* **6,** 308–316.

——, and Coauthors, 1995: Absorption of solar radiation by clouds: Observations versus models. *Science,* **267,** 496–499.

Coakley, J. A., R. D. Cess, and F. B. Yurevich, 1983: The effect of tropospheric aerosols on the earth's radiation budget: A parameterization for climate models. *J. Atmos. Sci.,* **40,** 116–138.

Collins, W. D., F. P. J. Valero, P. J. Flatau, D. Lubin, H. Grassl, P. Pilewskie, and J. Spinhirne, 1996: The radiative effects of convection in the tropical Pacific. *J. Geophys. Res.,* **101,** 14 999–15 012.

Conant, W. C., 1996: An examination of the solar absorption under clear skies for the central equatorial Pacific: Observations versus models. M.S. thesis, Scripps Institution of Oceanography, University of California, 50 pp. [Available from Center for Clouds, Chemistry and Climate, University of California, San Diego, CA 92093-0239.]

Li, Z., H. G. Leighton, K. Masuda, and T. Takashima, 1993a: Estimation of SW flux Absorbed at the surface from TOA reflected flux. *J. Climate,* **6,** 317–330.

——, ——, and R. D. Cess, 1993b: Surface net solar radiation estimated from satellite measurements: Comparisons with tower observations. *J. Climate,* **6,** 1764–1772.

——, H. W. Barker, and L. Moreau, 1995: The variable effect of clouds on atmospheric solar radiation. *Nature,* **376,** 486–490.

Michalsky, J. J., 1988: The *Astronomical Almanac's* algorithm for approximate solar position (1950–2050). *Sol. Energy,* **40,** 227–235.

Ohmura, A., and H. Gilgen, 1993: Re-evaluation of the global energy balance. *Interactions between Global Climate Systems, the Legacy of Hann, Geophys. Monogr.,* No. 75, IUGG, 93–110.

Pilewskie, P., and F. P. J. Valero, 1995: Direct observations of excess solar absorption by clouds. *Science,* **267,** 1626–1628.

Ramanathan, V., R. D. Cess, E. F. Harrison, P. Minnis, B. R. Barkstrom, E. Ahmad, and D. Hartmann, 1989: Cloud-radiative forcing and climate: Results from the Earth Radiation Budget Experiment. *Science,* **243,** 57–63.

——, B. Subasilar, G. Zhang, W. Conant, R. D. Cess, J. Kiehl, H. Grassl, and L. Shi, 1995: Warm pool heat budget and shortwave cloud forcing: A missing physics? *Science,* **267,** 499–503.

Shettle, E. P., and R. W. Fenn, 1979: Models for the aerosols of the lower atmosphere and the effects of humidity variations on their optical properties. Air Force Geophysics Laboratory Rep. AFGL-TR-79-0214, 94 pp. [Available from AFGL (OP), Hanscom AFB, MA 01731.]

Shi, L., 1994: Cloud radiative forcing on surface shortwave fluxes: A case study based on cloud lidar and radar exploratory test. *J. Geophys. Res.,* **99,** 25 909–25 919.

Spencer, J. W., 1989: Comments on *Astronomical Almanac's* algorithm for approximate solar position (1950–2050). *Sol. Energy,* **42,** 353.

Stamnes, K., S. C. Tsay, W. J. Wiscombe, and K. Jayaweera, 1988: Numerically stable algorithms for discrete-ordinate-method radiative transfer in multiple scattering and emitting layered media. *Appl. Opt.,* **27,** 2502–2509.

Stephens, G. L., 1996: How much solar radiation do clouds absorb? *Science,* **271,** 1131–1136.

——, and S. Tsay, 1990: On the cloud absorption anomaly. *Quart. J. Roy. Meteor. Soc.,* **116,** 671–704.

Valero, F. P. J., and P. Pilewskie, 1992: Latitudinal survey of spectral optical depths of the Pinatubo volcanic cloud—Derived particle sizes, columnar mass loadings, and effects on planetary albedo. *Geophys. Res. Lett.,* **19,** 163–166.

Weaver, C. P., W. D. Collins, and H. Grassl, 1994: Relationship between clear-sky atmospheric greenhouse effect and deep convection during the Central Equatorial Pacific Experiment: Model calculations and satellite observations. *J. Geophys. Res.,* **99,** 25 891–25 901.

Wild, M., A. Ohmura, H. Gilgen, and E. Roeckner, 1995: Validation of GCM radiative fluxes using surface observations. *J. Climate,* **8,** 1309–1324.